

Symmetry-breaking magnetization dynamics of spinor dipolar Bose-Einstein condensates

Shoichi Hoshi and Hiroki Saito

Department of Applied Physics and Chemistry, The University of Electro-Communications, Tokyo 182-8585, Japan

(Dated: June 17, 2021)

Symmetry-breaking magnetization dynamics of a spin-1 Bose-Einstein condensate (BEC) due to the dipole-dipole interaction are investigated using the mean-field and Bogoliubov theories. When a magnetic field is applied along the symmetry axis of a pancake-shaped BEC in the $m = 0$ hyperfine sublevel, transverse magnetization develops breaking the chiral or axial symmetry. A variety of magnetization patterns are formed depending on the strength of the applied magnetic field. The proposed phenomena can be observed in ^{87}Rb and ^{23}Na condensates.

PACS numbers: 03.75.Mn,67.85.Fg,03.75.Lm,03.75.Kk

I. INTRODUCTION

A Bose-Einstein condensate (BEC) of atoms with spin degrees of freedom (spinor BEC) allows the study of magnetism in a quantum fluid. There are two mechanisms of magnetization for a spinor BEC: the ferromagnetic contact interaction and the magnetic dipole interaction (MDI) between atoms. Magnetization dynamics due to the ferromagnetic contact interaction have been observed for a spin-1 ^{87}Rb BEC [1, 2]. However, magnetization dynamics due to the MDI have not been studied yet, and this is the subject of the present paper.

A BEC of ^{52}Cr atoms with a large magnetic dipole moment ($6 \mu_B$ with μ_B being the Bohr magneton) has been realized by the Stuttgart group [3] and its anisotropic behaviors originating from the anisotropy of the dipole-dipole interaction have been observed [4, 5, 6, 7, 8]. While the magnetic dipole moment of spin-1 alkali atoms ($\mu_B/2$) is much smaller than that of ^{52}Cr , it is nevertheless predicted that a small MDI can create spin textures in a ^{87}Rb BEC [9, 10, 11]. The crystalline magnetic order observed in a ^{87}Rb BEC is considered to be caused by the MDI [12]. MDI effects have been detected in ^{39}K [13] and ^7Li [14] BECs using Feshbach resonance.

In this paper, we show that magnetization dynamically develops in spin-1 ^{87}Rb and ^{23}Na BECs due to the MDI. We consider a situation in which a BEC in the $m = 0$ magnetic sublevel is confined in an axisymmetric pancake-shaped trap and a magnetic field is applied along the symmetry axis. We numerically solve the time-dependent nonlocal Gross-Pitaevskii (GP) equation including the MDI and show that magnetization develops in the direction perpendicular to the magnetic field due to the MDI. These magnetization dynamics break the chiral or axial symmetry spontaneously. We find that various magnetization patterns emerge depending on the strength of the magnetic field. For spin-1 ^{87}Rb , we can suppress magnetization due to the ferromagnetic contact interaction using the microwave-induced quadratic Zeeman effect [15], and the pure MDI effect can thus be observed. We perform a Bogoliubov analysis and show that the magnetization is triggered by the dynamical in-

stability. We also employ the variational method with the Gaussian approximation to explain the numerical results.

This paper is organized as follows. Section II formulates the mean-field and Bogoliubov theories to study the present system. Section III numerically studies the Bogoliubov spectra and demonstrates the magnetization dynamics. Section IV analyzes the phenomena using the variational method. Section V gives conclusions to the study.

II. FORMULATION OF THE PROBLEM

A. Mean-field theory

We consider a system of spin-1 bosonic atoms with mass M and magnetic dipole moment $\mu_B/2$ confined in an axisymmetric harmonic potential $V(\mathbf{r}) = M(\omega_\perp^2 r_\perp^2 + \omega_z^2 z^2)/2$ with $r_\perp = (x^2 + y^2)^{1/2}$. A uniform magnetic field B_z is applied in the z direction and the linear Zeeman energy is given by $-\mu_B B_z m/2$ for magnetic sublevels $m = 0, \pm 1$. We neglect the magnetic quadratic Zeeman effect, since the strength of the magnetic field considered here is $B_z < 10$ mG. Instead, we assume that the microwave-induced quadratic Zeeman effect [15] lifts the energy of the $m = \pm 1$ states by Q .

We employ the mean-field approximation and the condensate is described by the macroscopic wave function ψ_m with magnetic sublevel m , which satisfies the normalization condition $\sum_m \int |\psi_m|^2 d\mathbf{r} = N$, with N being the total number of atoms. The nonlocal GP equations including the MDI are given by

$$i\hbar \frac{\partial \psi_0}{\partial t} = \left(-\frac{\hbar^2}{2M} \nabla^2 + V + g_0 \rho \right) \psi_0 + \frac{g_1}{\sqrt{2}} (F_+ \psi_1 + F_- \psi_{-1}) - \frac{\mu_B}{2} B_d \cdot \sum_m (\mathbf{f})_{0m} \psi_m, \quad (1a)$$

$$\begin{aligned}
i\hbar \frac{\partial \psi_{\pm 1}}{\partial t} &= \left(-\frac{\hbar^2}{2M} \nabla^2 + V \mp P + Q + g_0 \rho \right) \psi_{\pm 1} \\
&+ g_1 \left(\frac{1}{\sqrt{2}} F_{\mp} \psi_0 \pm F_z \psi_{\pm 1} \right) - \frac{\mu_B}{2} \mathbf{B}_d \cdot \sum_m (\mathbf{f})_{\pm 1 m} \psi_m,
\end{aligned} \tag{1b}$$

where $\rho = \sum_m |\psi_m|^2$, $\mathbf{F} = \sum_{mm'} \psi_m^* (\mathbf{f})_{mm'} \psi_{m'}$, \mathbf{f} is the vector of the spin-1 matrices, $F_{\pm} = F_x \pm iF_y$, and

$$P = \frac{\mu_B}{2} B_z. \tag{2}$$

The spin-independent and spin-dependent contact-interaction parameters g_0 and g_1 have the forms

$$g_0 = \frac{4\pi\hbar^2}{M} \frac{a_0 + 2a_2}{3}, \quad g_1 = \frac{4\pi\hbar^2}{M} \frac{a_2 - a_0}{3}, \tag{3}$$

where a_S is the s -wave scattering length for colliding atoms with total spin S . The MDI produces an effective magnetic field:

$$\mathbf{B}_d(\mathbf{r}) = -\frac{\mu_0}{4\pi} \frac{\mu_B}{2} \int d\mathbf{r}' \frac{\mathbf{F}(\mathbf{r}') - 3[\mathbf{F}(\mathbf{r}') \cdot \mathbf{e}]\mathbf{e}}{|\mathbf{r} - \mathbf{r}'|^3}, \tag{4}$$

where μ_0 is the magnetic permeability of vacuum and $\mathbf{e} = (\mathbf{r} - \mathbf{r}')/|\mathbf{r} - \mathbf{r}'|$. Equation (1) is numerically solved in Fourier space for the kinetic term and in real space for the other terms using a fast Fourier transform (FFT). The FFT is also used to calculate the convolution integral in Eq. (4).

In the present paper, we consider an initial state in which all the atoms are in the $m = 0$ sublevel. In order to simulate this situation, we prepare the ground state of ψ_0 with $\psi_{\pm 1} = 0$ by the imaginary-time evolution of Eq. (1). Small noise (a complex random number on each mesh) is then applied to the initial state of $\psi_{\pm 1}$ to break the symmetry and trigger magnetization due to dynamical instability. The small noise corresponds to quantum fluctuation, thermal atoms, and residual atoms in an experiment. We note that if the initial state of $m = \pm 1$

is $\psi_{\pm 1} = 0$, the right-hand side of Eq. (1b) vanishes and $\psi_{\pm 1}$ never develops within the mean-field theory. Magnetization thus occurs if small noise in the $m = \pm 1$ state is exponentially amplified by dynamical instabilities.

B. Bogoliubov analysis

We investigate the Bogoliubov excitation spectrum of magnons for the stationary state of ψ_0 . Assuming that $\psi_{\pm 1}$ is small and neglecting the second and higher orders of $\psi_{\pm 1}$ in Eq. (1), we obtain

$$\begin{aligned}
i\hbar \frac{\partial \psi_{\pm 1}}{\partial t} &= \left(-\frac{\hbar^2}{2M} \nabla^2 + V \mp P + Q + g_0 |\psi_0|^2 \right) \psi_{\pm 1} \\
&+ g_1 (|\psi_0|^2 \psi_{\pm 1} + \psi_0^2 \psi_{\mp 1}^*) - \frac{g_d}{2\sqrt{2}} \int d\mathbf{r}' \frac{1}{|\mathbf{r} - \mathbf{r}'|^3} \\
&\times [(1 - 3e_z^2) F_{\mp}(\mathbf{r}') + 3e_{\mp}^2 F_{\pm}(\mathbf{r}')] \psi_0(\mathbf{r}),
\end{aligned} \tag{5}$$

where $g_d = \mu_0 \mu_B^2 / (16\pi)$ and $e_{\pm} = e_x \pm ie_y$. Using the mode functions $u_{\pm 1}$ and $v_{\pm 1}$, we write a single-mode excitation of $\psi_{\pm 1}$ as

$$\begin{aligned}
\psi_{\pm 1}(\mathbf{r}, t) &= e^{-i\mu t/\hbar} \left[u_{\pm 1}(r_{\perp}, z) e^{i(L\pm 1)\phi} e^{-i\omega t} \right. \\
&\quad \left. + v_{\pm 1}^*(r_{\perp}, z) e^{-i(L\mp 1)\phi} e^{i\omega t} \right],
\end{aligned} \tag{6}$$

where $\phi = \arg(x + iy)$, L is an integer, and μ is the chemical potential,

$$\mu = \frac{1}{N} \int d\mathbf{r} \psi_0^* \left(-\frac{\hbar^2}{2M} \nabla^2 + V + g_0 |\psi_0|^2 \right) \psi_0. \tag{7}$$

Each $\psi_{\pm 1}$ in Eq. (6) has $2(L - 1)$ -fold symmetry around the z axis. Substituting Eq. (6) and $\psi_0 = |\psi_0| \exp(-i\mu t/\hbar)$ into Eq. (5) yields the closed form of the nonlocal Bogoliubov-de Gennes equations,

$$\begin{aligned}
&\left\{ -\frac{\hbar^2}{2M} \left[\nabla_{\perp z}^2 - \frac{(L \pm 1 - 1)^2}{r_{\perp}^2} \right] + V \mp P + Q + g_0 |\psi_0|^2 - \mu \right\} u_{\pm 1} + g_1 |\psi_0|^2 (u_{\pm 1} + v_{\mp 1}) \\
&- \frac{g_d}{2} \int d\mathbf{r}' \frac{|\psi_0(\mathbf{r}')|}{|\mathbf{r} - \mathbf{r}'|^3} \left\{ (1 - 3e_z^2) [u_{\pm 1}(\mathbf{r}') + v_{\mp 1}(\mathbf{r}')] + 3e_{\mp}^2 [u_{\mp 1}(\mathbf{r}') + v_{\pm 1}(\mathbf{r}')] \right\} |\psi_0(\mathbf{r})| = \hbar\omega u_{\pm 1},
\end{aligned} \tag{8a}$$

$$\begin{aligned}
&\left\{ -\frac{\hbar^2}{2M} \left[\nabla_{\perp z}^2 - \frac{(L \mp 1 - 1)^2}{r_{\perp}^2} \right] + V \mp P + Q + g_0 |\psi_0|^2 - \mu \right\} v_{\pm 1} + g_1 |\psi_0|^2 (u_{\mp 1} + v_{\pm 1}) \\
&- \frac{g_d}{2} \int d\mathbf{r}' \frac{|\psi_0(\mathbf{r}')|}{|\mathbf{r} - \mathbf{r}'|^3} \left\{ (1 - 3e_z^2) [u_{\mp 1}(\mathbf{r}') + v_{\pm 1}(\mathbf{r}')] + 3e_{\pm}^2 [u_{\pm 1}(\mathbf{r}') + v_{\mp 1}(\mathbf{r}')] \right\} |\psi_0(\mathbf{r})| = -\hbar\omega v_{\pm 1},
\end{aligned} \tag{8b}$$

where $\nabla_{\perp z}^2 = \partial_{r_{\perp}}^2 + r_{\perp}^{-1} \partial_{r_{\perp}} + \partial_z^2$. We numerically diagonalize Eq. (8) by expanding $u_{\pm 1}$ and $v_{\pm 1}$ with orthog-

onal bases, e.g., the harmonic-oscillator eigenfunctions.

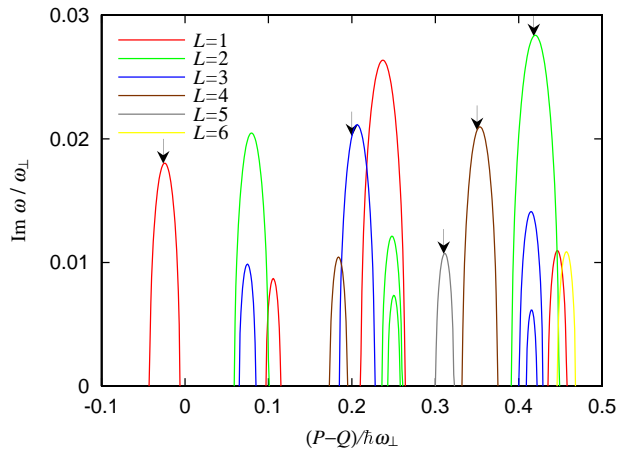


FIG. 1: (color) Imaginary part of Bogoliubov frequency ω for magnon excitation from the $m = 0$ state of ^{87}Rb atoms as a function of $P - Q$ with $Q = 50\hbar\omega_{\perp}$. The excitation mode has $2(L - 1)$ -fold symmetry around the z axis, where L is defined in Eq. (6). The number of atoms is $N = 10^5$ and the radial and axial trap frequencies are $\omega_{\perp} = 2\pi \times 100$ Hz and $\omega_z = 2\pi \times 400$ Hz. The values of P indicated by the arrows are used in Figs. 2 and 3.

If complex frequencies ω emerge, the stationary state ψ_0 becomes dynamically unstable against excitations of magnons.

III. MAGNETIZATION DYNAMICS AND BOGOLIUBOV SPECTRA FOR ALKALI ATOMS

A. Spin-1 rubidium 87

We first consider a spin-1 ^{87}Rb BEC. The scattering lengths are $a_0 = 101.8a_B$ and $a_2 = 100.4a_B$ [16] with a_B being the Bohr radius. The spin-dependent contact-interaction parameter g_1 is therefore negative and the ground state is ferromagnetic [1]. In order to distinguish magnetization by the MDI from that by the ferromagnetic contact interaction, we apply microwave radiation to lift the energy of the $m = \pm 1$ states by Q , which must be much larger than the ferromagnetic interaction energy $|g_1|\rho$. The magnetization due to the ferromagnetic contact interaction is thus suppressed and the pure effect of the MDI can be observed.

To investigate the dynamical instability against magnetization, we numerically diagonalize Eq. (8). Figure 1 shows the imaginary part of the Bogoliubov frequencies ω as a function of the applied magnetic field, where $N = 10^5$ atoms are confined in a pancake-shaped trap with $\omega_{\perp} = 2\pi \times 100$ Hz and $\omega_z = 2\pi \times 400$ Hz. The microwave-induced quadratic Zeeman energy Q is chosen to be $50\hbar\omega_{\perp}$, which is sufficient to suppress magnetization by the ferromagnetic contact interaction. In fact, we have confirmed that the Bogoliubov spectrum is always real if the MDI is absent, $g_d = 0$, for this

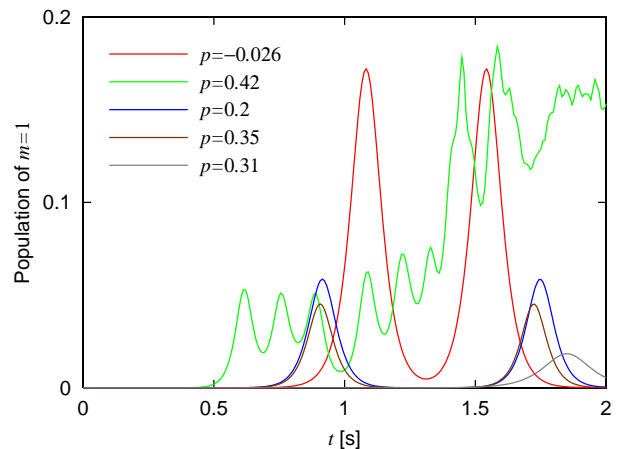


FIG. 2: (color) Time evolution of the population of the $m = 1$ state $\int |\psi_1|^2 d\mathbf{r} / N$ for the values of $p \equiv (P - Q) / (\hbar\omega_{\perp})$ indicated by the arrows in Fig. 1. The parameters are the same as those in Fig. 1. The populations of the $m = -1$ state are too small to be discerned at this scale of the ordinate.

value of Q . The linear Zeeman energy $P = 50\hbar\omega_{\perp}$ corresponds to $B_z \simeq 7.15$ mG. From Fig. 1, we find that magnon modes with various rotational symmetries (various L) become dynamically unstable, depending on the linear Zeeman energy P . There is no imaginary part for $p \equiv (P - Q) / (\hbar\omega_{\perp}) < -0.1$, while many peaks in the imaginary part exist for $p > 0.5$.

Figure 2 shows time evolution of $\int |\psi_1|^2 d\mathbf{r} / N$ for the values of P indicated by the arrows in Fig. 1. The transition from the $m = 0$ state to the $m = 1$ state occurs due to the dynamical instability shown in Fig. 1. From Fig. 2, we find that the transition occurs periodically except for $p = 0.42$ (green line). The complicated behavior for $p = 0.42$ originates from the fact that the dynamically unstable modes are not only $L = 2$ but also $L = 3$ (see Fig. 1). We note that the transition to the $m = -1$ state is negligibly small and the total spin in the z direction $\int (|\psi_1|^2 - |\psi_{-1}|^2) d\mathbf{r}$ is not conserved, indicating that the transition is not due to the spin-exchange contact interaction but due to the MDI. Since the z component of the total angular momentum must be conserved, the system acquires orbital angular momentum. The transfer of the spin angular momentum to the orbital angular momentum in a spinor dipolar BEC also occurs in the Einstein-de Haas effect [17, 18, 19].

Figure 3 shows transverse magnetization at the times of the first peaks of $\int |\psi_1|^2 d\mathbf{r}$ (the first peaks of the lines in Fig. 2) for the linear Zeeman energies P indicated by the arrows in Fig. 1. A variety of magnetization patterns with $2(L - 1)$ -fold symmetry emerge depending on the strength of the applied magnetic field. The closure structure of the magnetization in Fig. 2 (a) is an energetically favorable structure for the MDI energy. The directions of the magnetization vectors in the closure structure have clockwise and counterclockwise symmetry, and therefore the spin-vortex generation in Fig. 3 (a) breaks the chiral

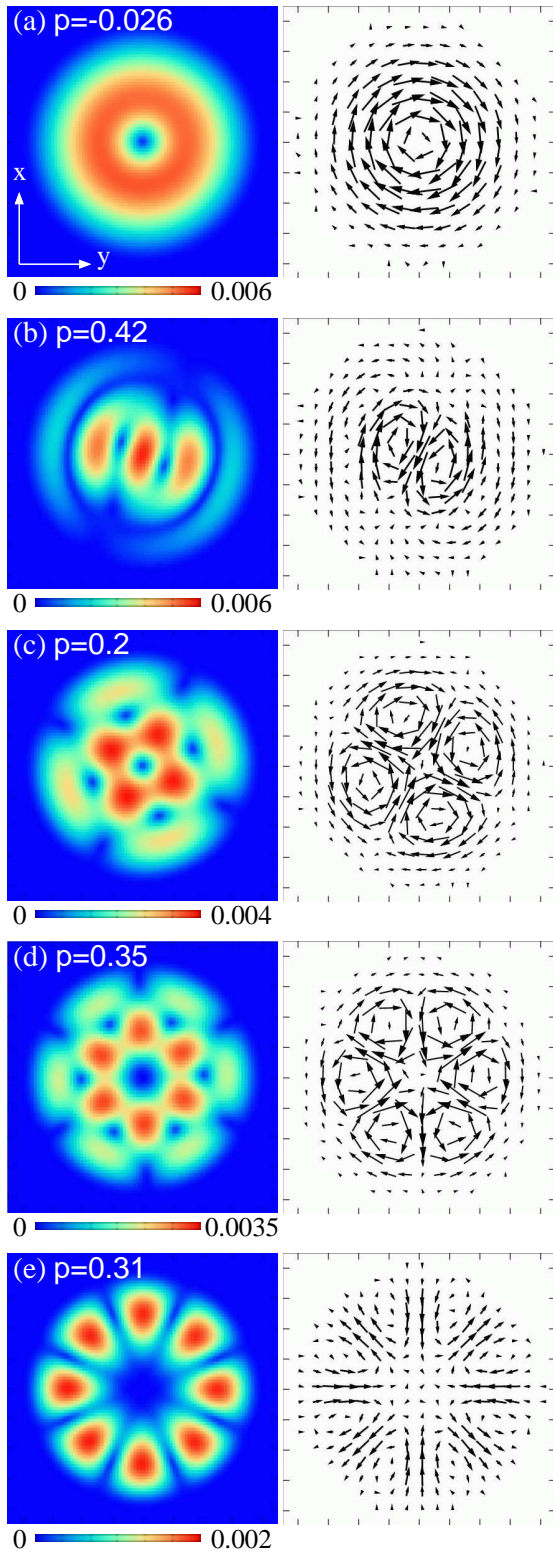


FIG. 3: (color) Magnitude of the integrated transverse magnetization $|\int F_+ dz|$ (right panels) and its direction $\arg(\int F_+ dz)$ (left panels) at the first peaks of the curves in Fig. 2. The values of $p \equiv (P - Q)/(\hbar\omega_\perp)$ used are indicated by the arrows in Fig. 1. The unit of $\int F_+ dz$ is $NM\omega_\perp/\hbar$. The length of the vector is proportional to $|\int F_+ dz|$. The field of view is $9.7 \times 9.7 \mu\text{m}$.

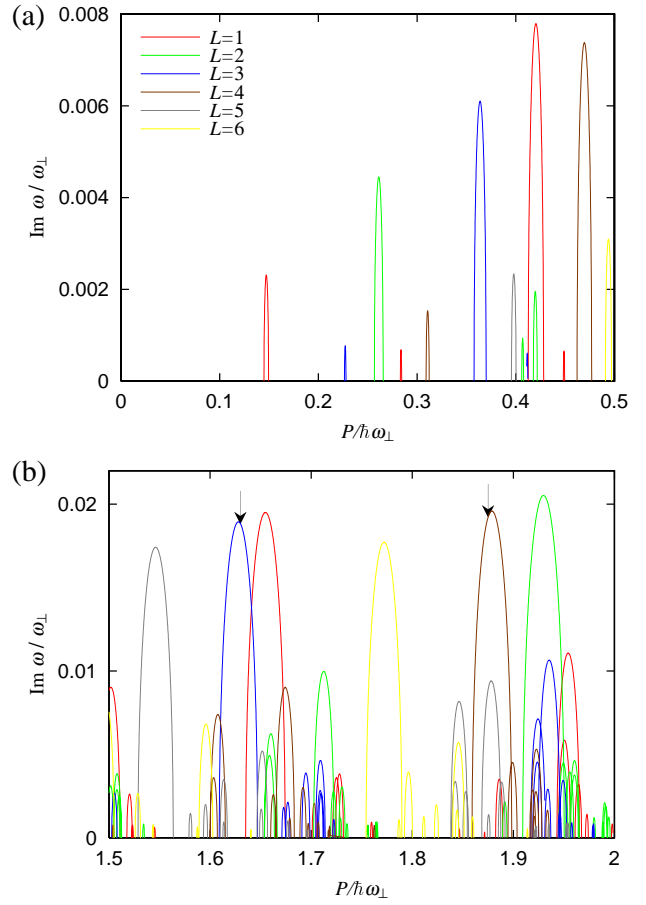


FIG. 4: (color) Imaginary part of the Bogoliubov frequency ω for magnon excitation from the $m = 0$ state of ^{23}Na atoms as a function of the linear Zeeman energy P . The range of P is (a) $0 \leq P/(\hbar\omega_\perp) \leq 0.5$ and (b) $1.5 \leq P/(\hbar\omega_\perp) \leq 2$. The excitation mode has $2(L - 1)$ -fold symmetry around the z axis, where L is defined in Eq. (6). The number of atoms is $N = 10^6$ and the trap frequencies are the same as those in Fig. 1. The values of P indicated by the arrows in (b) are used in Fig. 5.

symmetry. The $m = 1$ component of these spin vortices is $\psi_1 \propto e^{-i\phi}$. This situation is different from the spin-vortex generation by the ferromagnetic contact interaction, in which polar-core vortices of $\psi_{\pm 1} \propto e^{\pm i\phi}$ and $\psi_{\pm 1} \propto e^{\mp i\phi}$ emerge with an equal probability [20]. The closure structures are also seen in Figs. 3 (b)-3 (e). The magnetization in Figs. 3 (b)-3 (e) caused by the dynamical instability with $L \geq 1$ exhibits a variety of patterns, breaking the axisymmetry of the system.

B. Spin-1 sodium 23

Next we consider a spin-1 ^{23}Na BEC. The scattering lengths are given by $(a_0 + 2a_2)/3 = 53.4a_B$ [21] and $a_2 - a_0 = 2.47a_B$ [22]. The spin-dependent contact-interaction parameter g_1 is then positive and the polar

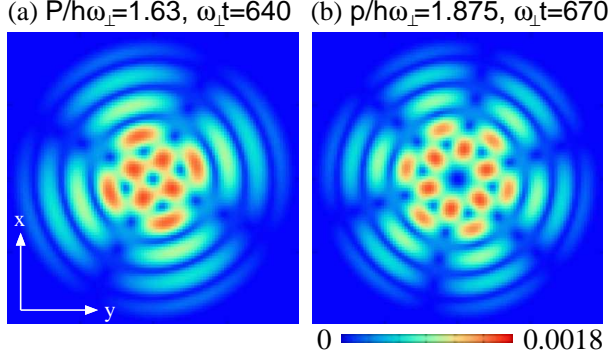


FIG. 5: (color) Integrated transverse magnetization $|\int F_+ dz|$ at the time when $\int |\psi_1|^2 d\mathbf{r}$ becomes the first maximum in time evolution for the values of P indicated by the arrows in Fig. 4 (b). The unit of $|\int F_+ dz|$ is $NM\omega_\perp/\hbar$. The field of view is $21 \times 21 \mu\text{m}$.

state ($m = 0$) is energetically favorable. Spontaneous magnetization due to the contact interaction is therefore suppressed and the microwave-induced Zeeman effect is unnecessary ($Q = 0$). The number of atoms is assumed to be $N = 10^6$ and the trap frequencies are the same as those in Sec. III A.

Figure 4 shows the imaginary part of the Bogoliubov frequency obtained by numerically diagonalizing Eq. (8). Compared with the case of ^{87}Rb in Fig. 1, the width and height of the peaks are small for $0 \leq P/(\hbar\omega_\perp) \leq 0.5$ [Fig. 4 (a)]. The width and height of the main peaks gradually increase and saturate for $P/(\hbar\omega_\perp) \sim 2$ [Fig. 4 (b)]. For $P < 0$, there is no imaginary part.

We numerically solve the GP equation for the values of P indicated by the arrows in Fig. 4 (b). The initial state is prepared by the same method as for ^{87}Rb . Figure 5 shows the integrated transverse magnetization $|\int F_+ dz|$ at the time of the first peak of $\int |\psi_1|^2 d\mathbf{r}$ in the time evolution. Many radial nodes in the magnetization patterns are evident, since the values of P correspond to the higher-order peaks in Fig. 4 (b). The population of the $m = 1$ state, $\int |\psi_1|^2 d\mathbf{r}/N$, is 0.01 in Fig. 5 (a) and 0.05 in Figure 5 (b). The population of the $m = -1$ state is very small $\sim 10^{-4}$.

IV. GAUSSIAN VARIATIONAL ANALYSIS

To qualitatively examine the Bogoliubov spectra obtained in Sec. III, we perform Gaussian variational analysis. The variational wave function for the $m = 0$ state has the form

$$\psi_0 = \frac{\sqrt{N}}{\pi^{3/4} d_\perp d_z^{1/2}} \exp\left(-\frac{r_\perp^2}{2d_\perp^2} - \frac{z^2}{2d_z^2} - i\frac{\mu}{\hbar}t\right), \quad (9)$$

where d_\perp and d_z are the variational parameters characterizing the size of the condensate in the radial and axial directions. Substituting Eq. (9) into Eq. (7) and

the mean-field energy

$$E = \int d\mathbf{r} \psi_0^* \left(-\frac{\hbar^2}{2M} \nabla^2 + V + \frac{g_0}{2} |\psi_0|^2 \right) \psi_0, \quad (10)$$

we obtain

$$\frac{\mu}{\hbar\omega_\perp} = \frac{1}{2} \left(\frac{1}{\tilde{d}_\perp^2} + \tilde{d}_\perp^2 \right) + \frac{1}{4} \left(\frac{1}{\tilde{d}_z^2} + \lambda^2 \tilde{d}_z^2 \right) + \frac{\tilde{g}_0}{\tilde{d}_\perp^2 \tilde{d}_z}, \quad (11)$$

$$\frac{E}{N\hbar\omega_\perp} = \frac{1}{2} \left(\frac{1}{\tilde{d}_\perp^2} + \tilde{d}_\perp^2 \right) + \frac{1}{4} \left(\frac{1}{\tilde{d}_z^2} + \lambda^2 \tilde{d}_z^2 \right) + \frac{\tilde{g}_0}{2\tilde{d}_\perp^2 \tilde{d}_z}, \quad (12)$$

where $\lambda = \omega_z/\omega_\perp$, $\tilde{d}_\perp = d_\perp/a_\perp$, $\tilde{d}_z = d_z/a_\perp$, and $\tilde{g}_0 = g_0 N / [(2\pi)^{3/2} \hbar \omega_\perp a_\perp^3]$ with $a_\perp = [\hbar/(M\omega_\perp)]^{1/2}$. The variational parameters \tilde{d}_\perp and \tilde{d}_z are determined so as to minimize Eq. (12).

For simplicity, we restrict the magnon excitation to the form,

$$\psi_{\pm 1}(\mathbf{r}, t) = e^{-i\mu t/\hbar} [\alpha_{\pm 1} e^{-i\omega t} \chi_{\pm}(\mathbf{r}) + \beta_{\pm 1}^* e^{i\omega t} \chi_{\mp}(\mathbf{r})], \quad (13)$$

with

$$\chi_{\pm}(\mathbf{r}) = \frac{e^{\pm i\phi} r_\perp}{\pi^{3/4} d_\perp^2 d_z^{1/2}} \exp\left(-\frac{r_\perp^2}{2d_\perp^2} - \frac{r_z^2}{2d_z^2}\right), \quad (14)$$

which corresponds to the lowest mode of $L = 1$ in Eq. (6). Substitution of Eqs. (9), (11), and (13) into Eq. (8) yields

$$(\Lambda \mp \tilde{P})\alpha_{\pm 1} + (G + D_1)(\alpha_{\pm 1} + \beta_{\mp 1}) + D_2(\alpha_{\mp 1} + \beta_{\pm 1}) = \tilde{\omega}\alpha_{\pm 1}, \quad (15a)$$

$$(\Lambda \mp \tilde{P})\beta_{\pm 1} + (G + D_1)(\alpha_{\mp 1} + \beta_{\pm 1}) + D_2(\alpha_{\pm 1} + \beta_{\mp 1}) = -\tilde{\omega}\beta_{\pm 1}, \quad (15b)$$

where $\tilde{P} = P/(\hbar\omega_\perp)$, $\tilde{\omega} = \omega/\omega_\perp$, and

$$\Lambda = \frac{1}{2} \left(\frac{1}{\tilde{d}_\perp^2} + \tilde{d}_\perp^2 \right) + \frac{Q}{\hbar\omega_\perp} - \frac{\tilde{g}_0}{2\tilde{d}_\perp^2 \tilde{d}_z}, \quad (16)$$

$$G = \frac{Ng_1}{2(2\pi)^{3/2} \hbar \omega_\perp a_\perp^3 \tilde{d}_\perp^2 \tilde{d}_z}, \quad (17)$$

$$D_1 = \frac{\tilde{g}_d}{2\tilde{d}_\perp^2 \tilde{d}_z (\tilde{d}_\perp^2 - \tilde{d}_z^2)^{5/2}} \times \left[(\tilde{d}_\perp^2 - \tilde{d}_z^2)^{1/2} (-4\tilde{d}_\perp^4 - 7\tilde{d}_\perp^2 \tilde{d}_z^2 + 2\tilde{d}_z^4) + 9\tilde{d}_\perp^4 \tilde{d}_z \cot^{-1} \frac{\tilde{d}_z}{(\tilde{d}_\perp^2 - \tilde{d}_z^2)^{1/2}} \right], \quad (18)$$

$$D_2 = \frac{3\tilde{g}_d}{2\tilde{d}_\perp^2 (\tilde{d}_\perp^2 - \tilde{d}_z^2)^{5/2}} \left[\tilde{d}_z (\tilde{d}_\perp^2 - \tilde{d}_z^2)^{1/2} (-5\tilde{d}_\perp^2 + 2\tilde{d}_z^2) + 3\tilde{d}_\perp^4 \cot^{-1} \frac{\tilde{d}_z}{(\tilde{d}_\perp^2 - \tilde{d}_z^2)^{1/2}} \right], \quad (19)$$

with $\tilde{g}_d = g_d N / [6(2\pi)^{1/2} \hbar \omega_{\perp} a_{\perp}^3]$. Diagonalizing Eq. (15), we obtain the excitation frequency as

$$\tilde{\omega}^2 = \tilde{P}^2 + \Lambda^2 + 2(G + D_1)\Lambda \pm 2\sqrt{[\Lambda^2 + 2(G + D_1)\Lambda]\tilde{P}^2 + \Lambda^2 D_2^2}. \quad (20)$$

For the parameters of ^{87}Rb in Fig. 1, $\tilde{\omega}$ in Eq. (20) becomes imaginary between $\tilde{P} \simeq 49.9$ and 50.01 and the maximum value of $\text{Im } \omega$ is $\simeq 0.01$. For the parameters of ^{23}Na in Fig. 4, $\tilde{\omega}$ becomes imaginary between $\tilde{P} \simeq 0.125$ and 0.13 and the maximum value of $\text{Im } \omega$ is $\simeq 0.002$. These results are in qualitative agreement with the first peaks of $L = 1$ in Figs. 1 and 4. The differences between the variational and numerical results come from the forms of the variational wave functions assumed in Eqs. (9) and (13); more appropriate variational functions are needed for quantitative explanation of the numerical results.

V. CONCLUSIONS

In conclusion, we have studied the magnetization dynamics caused by the MDI in a spin-1 BEC in the $m = 0$ hyperfine state prepared in a pancake-shaped trap and

a magnetic field applied in the axial direction. We found that transverse magnetization develops due to the MDI breaking the chiral or axial symmetry, and a variety of magnetization patterns appear depending on the strength of the applied magnetic field. We showed that these phenomena occur in spin-1 ^{87}Rb and ^{23}Na BECs. We also performed Bogoliubov analysis and found that the initial fluctuations in the magnetization are exponentially amplified by the dynamical instability. A Gaussian variational analysis provided a qualitative explanation of the results.

Our study has shown that magnetization due to the MDI strongly depends on the shape of the system. Magnetization dynamics for various trapping potentials including cigar-shaped and lattice potentials merit further study.

Acknowledgments

This work was supported by the Ministry of Education, Culture, Sports, Science and Technology of Japan (Grants-in-Aid for Scientific Research, No. 17071005 and No. 20540388).

-
- [1] M. -S. Chang, C. D. Hamley, M. D. Barrett, J. A. Sauer, K. M. Fortier, W. Zhang, L. You, and M. S. Chapman, *Phys. Rev. Lett.* **92**, 140403 (2004).
 - [2] L. E. Sadler, J. M. Higbie, S. R. Leslie, M. Vengalattore, and D. M. Stamper-Kurn, *Nature (London)* **443**, 312 (2006).
 - [3] A. Griesmaier, J. Werner, S. Hensler, J. Stuhler, and T. Pfau, *Phys. Rev. Lett.* **94**, 160401 (2005).
 - [4] A. Griesmaier, J. Stuhler, T. Koch, M. Fattori, T. Pfau, and S. Giovanazzi, *Phys. Rev. Lett.* **97**, 250402 (2006).
 - [5] T. Lahaye, T. Koch, B. Fröhlich, M. Fattori, J. Metz, A. Griesmaier, S. Giovanazzi, and T. Pfau, *Nature (London)* **448**, 672 (2007).
 - [6] T. Koch, T. Lahaye, J. Metz, B. Fröhlich, A. Griesmaier, and T. Pfau, *Nature Phys.* **4**, 218 (2008).
 - [7] T. Lahaye, J. Metz, B. Fröhlich, T. Koch, M. Meister, A. Griesmaier, T. Pfau, H. Saito, Y. Kawaguchi, and M. Ueda, *Phys. Rev. Lett.* **101**, 080401 (2008).
 - [8] J. Metz, T. Lahaye, B. Fröhlich, A. Griesmaier, T. Pfau, H. Saito, Y. Kawaguchi, and M. Ueda, *New J. Phys.* **11**, 055032 (2009).
 - [9] S. Yi and H. Pu, *Phys. Rev. Lett.* **97**, 020401 (2006).
 - [10] Y. Kawaguchi, H. Saito, and M. Ueda, *Phys. Rev. Lett.* **97**, 130404 (2006).
 - [11] Y. Kawaguchi, H. Saito, and M. Ueda, *Phys. Rev. Lett.* **98**, 110406 (2007).
 - [12] M. Vengalattore, S. R. Leslie, J. Guzman, and D. M. Stamper-Kurn, *Phys. Rev. Lett.* **100**, 170403 (2008).
 - [13] M. Fattori, G. Roati, B. Deissler, C. D'Errico, M. Zaccanti, M. Jona-Lasinio, L. Santos, M. Inguscio, and G. Modugno, *Phys. Rev. Lett.* **101**, 190405 (2008).
 - [14] S. E. Pollack, D. Dries, M. Junker, Y. P. Chen, T. A. Corcovilos, and R. G. Hulet, *Phys. Rev. Lett.* **102**, 090402 (2009).
 - [15] S. R. Leslie, J. Guzman, M. Vengalattore, J. D. Sau, M. L. Cohen, and D. M. Stamper-Kurn, *Phys. Rev. A* **79**, 043631 (2009).
 - [16] E. G. M. van Kempen, S. J. J. M. F. Kokkelmans, D. J. Heinzen, and B. J. Verhaar, *Phys. Rev. Lett.* **88**, 093201 (2002).
 - [17] Y. Kawaguchi and H. Saito and M. Ueda, *Phys. Rev. Lett.* **96**, 080405 (2006).
 - [18] L. Santos and T. Pfau, *Phys. Rev. Lett.* **96**, 190404 (2006).
 - [19] K. Gawryluk, M. Brewczyk, K. Bongs, and M. Gajda, *Phys. Rev. Lett.* **99**, 130401 (2007).
 - [20] H. Saito, Y. Kawaguchi, and M. Ueda, *Phys. Rev. Lett.* **96**, 065302 (2006).
 - [21] A. Crubellier, O. Dulieu, F. Masnou-Seeuws, M. Elbs, H. Knöckel, and E. Tiemann, *Eur. Phys. J. D* **6**, 211 (1999).
 - [22] A. T. Black, E. Gomez, L. D. Turner, S. Jung, and P. D. Lett, *Phys. Rev. Lett.* **99**, 070403 (2007).